PERGAMON

International Journal of Heat and Mass Transfer 46 (2003) 469–480

International Journal of HEAT and MASS TRANSFER

www.elsevier.com/locate/ijhmt

Heat transfer predictions with a cubic k–ε model for axisymmetric turbulent jets impinging onto a flat plate

Bart Merci *, Erik Dick

Department of Flow, Heat and Combustion Mechanics, Ghent University, Sint Pietersnieuwstraat 41, B-9000 Gent, Belgium

Received 8 March 2002; received in revised form 8 July 2002

Abstract

Local heat transfer in turbulent axisymmetric jets, impinging onto a flat plate, is predicted with a cubic k–ε model. Both the constitutive law for the Reynolds stresses and the transport equation for the dissipation rate ε contribute to improved heat transfer predictions. The stagnation point value and the shape of the profiles of the Nusselt number are well predicted for different distances between the nozzle and the flat plate. Accurate flow field predictions, obtained with the presented turbulence model, are the basis for the quality of the heat transfer results. The influence of the nozzle–plate distance on the stagnation point Nusselt number, is also correctly captured. For a fixed nozzle–plate distance, the influence of the Reynolds number on the stagnation point heat transfer is correctly reproduced. Comparisons are made to experimental data and to results from a low-Reynolds standard k–ε model [1] and the v^2–f model [2].

1. Introduction

Prediction of turbulent heat transfer in impinging flow situations is of importance in many industrial applications. The local heat transfer, expressed in dimensionless terms as the local value of the Nusselt number, is an important technical quantity. Therefore, the numerical study of the convective heat transfer of a round turbulent jet, impinging onto a flat plate, is of high interest. Numerical simulations must yield reliable predictions. However, as illustrated by Behnia et al. [2,3], the heat transfer at the stagnation point is dramatically overpredicted by the standard k–ε model, with a constant turbulent Prandtl number. In this paper, this is confirmed for a low-Reynolds version of the k–ε model by Yang and Shih[1] (further 'YS').

With Durbin's v^2–f turbulence model [4], accurate results are obtained [2,3], but at the cost of two supplementary equations: a transport equation for v^2 and an elliptic equation for f. Consequently, this model is more time consuming than non-linear two-equation Eddy viscosity turbulence models. Moreover, it is less straightforward to use such a type of turbulence model in current commercial CFD packages, which may be seen as a purely practical argument in favour of k–ε turbulence models. As was illustrated by Craft et al. [5], accurate results can be obtained with a cubic k–ε model with constant turbulent Prandtl number. In their model, the transport equation for the dissipation rate ε is modified with the 'Yap' correction. However, the constitutive law in [5], relating the turbulent stresses to the local mean velocity gradients, contains a quadratic vorticity tensor term. This is a physically inconsistent term with respect to certain realizability conditions [6]. A complete discussion on this topic is found in [7]. Moreover, the model as described in [5] has been particularly tuned for the test cases in [5], so that the general accuracy of the model has not been guaranteed yet.

In this paper, accurate results are presented for heat transfer of round turbulent jets, impinging onto a flat plate, with a non-linear Eddy-viscosity model which has already been successfully applied to a number of completely different flows [7–9]. This guarantees a global quality of the model to some extent. Only in [9], the current formulation is exactly used. The differences with

* Corresponding author. Tel.: +32-9-264-33-14; fax: +32-9-264-35-86.

E-mail address: bart.merci@rug.ac.be (B. Merci).

0017-9310/03/$ - see front matter
PII: S0017-9310(02)00300-9

Nomenclature

c_p	specific heat capacity at constant pressure
D	nozzle diameter
k	turbulent kinetic energy
p	pressure
P_k	production of turbulence kinetic energy
P_r	Prandtl number
$\bar{q}$	heat flux vector
R_y	dimensionless distance from solid boundary $\left(=\frac{\rho\sqrt{ky}}{\mu}\right)$
S	strain rate $(=(2S_{ij}S_{ij})^{1/2})$
S_k	source term for k
S_ε	source term for ε
T	temperature
T_0	temperature at nozzle exit
T_w	temperature at flat plate
U_b	bulk velocity
$\bar{v}$	velocity vector
x_k	coordinate direction
y	normal distance from wall

Greek symbols

δ_{ij}	Kronecker delta
ε	dissipation rate
ε_{ijk}	permutation tensor
κ	molecular thermal conductivity
μ	molecular viscosity
μ_t	turbulent or 'Eddy' viscosity
ρ	density
τ_t	turbulence time scale
η	dimensionless strain rate $(=\tau_t(S+\Omega)^{1/2})$
Ω	(absolute) vorticity $(=(2\Omega_{ij}\Omega_{ij})^{1/2})$

the model as in [7,8] are mainly for free shear flows and for impinging flows. In [9], it is illustrated that the quality of the results in [7,8] is at least retained and often improved for all considered test cases. The model, which is in low-Reynolds formulation, differs from the YS model in two aspects: the constitutive law is non-linear, and the transport equation for ε is physically more correct. Both aspects contribute to the improved accuracy of the results. The constitutive law does not violate the realizability conditions of [6].

In the next section, the governing equations are presented. As in [2,3,5], the work done by the viscous and turbulent stresses is neglected in the energy equation. Also the contributions in the total enthalpy from the mean and turbulent kinetic energy, are neglected. In [10], this is justified. It is also confirmed there that, as pointed out in [2], the use of a variable turbulent Prandtl number does not significantly improve the results. Therefore, a constant turbulent Prandtl number is used here.

The model is described next. Attention is focused onto the specific parts of the model which lead to improved heat transfer prediction results.

Next, the numerical method is shortly described. A complete description of the second-order accurate discretization and the treatment of the higher order terms of the turbulence model, is given in [10].

Finally, results are presented for the heat transfer of a round turbulent jet, impinging onto a flat plate. The basic Reynolds number is $Re = 23000$, based on the nozzle diameter D and the bulk velocity U_b at the nozzle exit. Experimental data are available for the heat transfer [11–14] and the flow field [15]. The most extensive set of data is for a distance H between the nozzle and the plate, equal to $H = 2D$ and $6D$, so that most of the results are given for these configurations. Results are presented for the heat transfer and the flow field: accurate flow field predictions form the basis for good heat transfer predictions. The influence of the nozzle distance on the stagnation point heat transfer is considered, too, as well as the effect of the Reynolds number for a fixed nozzle–plate distance. It is shown that the present model leads to good results for the local heat transfer at the flat plate and that the flow field is accurately described. It is also shown that the influence of the distance between the nozzle and the plate, as well as the effect of the Reynolds number for a fixed nozzle–plate distance, is correctly captured.

2. Governing equations

The steady-state transport equations are

$$\begin{cases} \nabla.(\rho\bar{v}) = 0 \\ \nabla.(\rho\bar{v}\bar{v}) + \nabla p = \nabla.(\bar{\bar{\tau}}) \\ \nabla.(\rho T\bar{v}) = \nabla.(\bar{q}/c_p) \\ \nabla.(\rho k\bar{v}) = \nabla.\left[\left(\mu + \frac{\mu_t}{\sigma_k}\right)(\nabla k)\right] + S_k \\ \nabla.(\rho\varepsilon\bar{v}) = \nabla.\left[\left(\mu + \frac{\mu_t}{\sigma_\varepsilon}\right)(\nabla\varepsilon)\right] + S_\varepsilon \end{cases} \quad (1)$$

External forces (such as gravity) and internal heat sources are absent. All averaging symbols are omitted. Since ρ is variable, Favre averaging is used.

The stress tensor $\bar{\bar{\tau}}$ consists of a molecular and a turbulent part:

$$\bar{\bar{\tau}} = 2\mu S_{ij} + \bar{\bar{\tau}}^t, \quad (2)$$

with S_{ij} the strain rate tensor:

$$S_{ij} = \frac{1}{2}\left(\frac{\partial v_i}{\partial x_j} + \frac{\partial v_j}{\partial x_i}\right) - \frac{1}{3}\delta_{ij}\frac{\partial v_k}{\partial x_k}. \quad (3)$$

The turbulent stress tensor is defined in the next section.

The energy equation deserves some extra attention. In principle, this is an equation for total enthalpy. Neglecting the contributions of mean and turbulent kinetic energy and assuming a constant specific heat, the equation is rewritten in terms of mean temperature T. As in [2,3,5], the work done by the stress tensor is also neglected. In [10], this is justified.

The heat flux $\bar{q}$ consists of a molecular and a turbulent part:

$$\bar{q} = -\frac{\mu c_p}{Pr}\nabla T - \frac{\mu_t c_p}{Pr_t}\nabla T, \quad (4)$$

so that the linear gradient hypothesis is used for the turbulent heat flux. As pointed out in [2], a variable turbulent Prandtl number does not significantly improve the results. Therefore, a constant turbulent Prandtl number is used.

3. Model description

3.1. Transport equations

The importance of the ε transport equation is well recognized. In [7], a transport equation is presented which yields good results for wall-dominated flows. Also the correct rotation dependence is established. However, the model suffers from the plane jet–round jet anomaly. In [16], the anomaly is resolved, but the transport equation is only valid in high Reynolds number flow regions. Moreover, the equation is not rotation dependent, which is necessary in the limit of rapid rotation [6]. In [9], the equations are combined:

$$\frac{\partial}{\partial x_j}(\rho\varepsilon v_j) = (1-f_{R_y})c_{\varepsilon 1}\frac{P_k}{\tau_t} + f_{R_y}C_1 S\rho\varepsilon - c_{\varepsilon 2}f_2\frac{\rho\varepsilon}{\tau_t} + \frac{\partial}{\partial x_j}\left[\left(\mu + \frac{\mu_t}{\sigma_\varepsilon}\right)\frac{\partial\varepsilon}{\partial x_j}\right] + E + Y_c, \quad (5)$$

with $c_{\varepsilon 1} = 1.44$, P_k the production term for turbulent kinetic energy and τ_t the turbulent time scale:

$$\tau_t = \frac{k}{\varepsilon} + \sqrt{\frac{\mu}{\rho\varepsilon}}. \quad (6)$$

The blending function f_{R_y} is defined as

$$f_{R_y} = \frac{1}{2} + \frac{1}{2}\sin\left(\frac{\pi}{2}\min\left[\max(R_y/500 - 3; -1); 1\right]\right), \quad (7)$$

with $R_y = (\rho\sqrt{k}y)/\mu$, y being the normal distance from the nearest solid boundary. The blending function goes from 0 to 1 in the interval $R_y = 1000$–2000. The strain rate S is obtained from Eqs. (16) and (3) and the parameter C_1 is

$$C_1 = \max\left(0.43; \frac{Sk/\varepsilon}{5 + Sk/\varepsilon}\right). \quad (8)$$

The parameter $c_{\varepsilon 2}$ is

$$c_{\varepsilon 2} = \max\left(1.83 + \frac{0.075\tau_t\Omega_{abs}}{1+\tau_t^2 S^2};\ C_2 f_{R_y}\right), \quad (9)$$

with $C_2 = 1.9$ and Ω_{abs} determined as $\Omega_{abs} = (2\Omega_{ij,abs}\Omega_{ij,abs})^{1/2}$ from the absolute vorticity:

$$\Omega_{ij,abs} = \frac{1}{2}\left(\frac{\partial v_i}{\partial x_j} - \frac{\partial v_j}{\partial x_i}\right) - \varepsilon_{ijk}\Omega_k, \quad (10)$$

with Ω_k the rotation speed of the reference frame around the k-axis of a non-inertial frame. The damping function is $f_2 = 1 - 0.22\exp(-Re_t^2/36)$, with $Re_t = \rho k\tau_t/\mu$ the turbulent Reynolds number. The Eddy-viscosity is defined as

$$\mu_t = \rho f_\mu c_\mu k\tau_t, \quad (11)$$

where c_μ is defined in Eq. (18). The model constant is $\sigma_\varepsilon = 1.2$. The low-Reynolds source term is

$$E = -1.8(1-f_\mu)\left(\mu + \frac{\mu_t}{\sigma_\varepsilon}\right)\frac{\partial k}{\partial x_i}\frac{\partial\tau_t^{-1}}{\partial x_i}, \quad (12)$$

where f_μ is given by Eq. (24).

The final term in the ε-equation forms the most influential difference from the standard k–ε model with respect to heat transfer predictions in turbulent impinging jets. All other differences make the model suitable for a wide variety of flows [9], but this is not the topic of this paper. The final term is based on the 'Yap' correction [5]:

$$\begin{cases} S \leqslant 1.05\Omega : Y_c = 0 \\ S > 1.05\Omega : Y_c = 0.13(1-f_{R_y})\frac{k^2}{y^2}\max\left[\left(\frac{0.4k^{3/2}}{\varepsilon y} - 1\right); 0\right] \end{cases}. \quad (13)$$

The overprediction of turbulent kinetic energy, a typical feature of the standard k–ε model, is counteracted by this term. It is only added when streamline curvature has a destabilising effect on turbulence ($S > \Omega$). The factor 1.05 has been added in order to avoid numerical problems by alternatingly switching on and off Y_c in regions where $S \approx \Omega$. The factor $(1 - f_{R_y})$ has been introduced so that Y_c certainly becomes zero away from solid boundaries. This is, in principle, also assured by the factor $1/y^2$, but adding the factor $(1 - f_{R_y})$ improves the results for certain test cases.

3.2. Constitutive law

The constitutive law is

$$\frac{\overline{v_i'v_j'}}{k} = \frac{2}{3}\delta_{ij} - 2c_\mu f_\mu\tau_t S_{ij} + q_1\tau_t^2\left(S_{ik}S_{kj} - \frac{1}{3}\delta_{ij}S_{lm}S_{ml}\right) + (q_2 + q_1/6)\tau_t^2(\Omega_{ik}S_{kj} - S_{ik}S_{kj}) + c_1\tau_t^3(S_{mn}S_{nm} + \Omega_{mn}\Omega_{nm})S_{ij} + c_2\tau_t^3(\Omega_{ik}S_{kl}S_{lj} - S_{ik}S_{kl}\Omega_{lj}), \quad (14)$$

with S_{ij} from (3) and the vorticity tensor:

$$\Omega_{ij} = \frac{1}{2}\left(\frac{\partial v_i}{\partial x_j} - \frac{\partial v_j}{\partial x_i}\right) - \varepsilon_{ijk} C_\Omega \Omega_k, \tag{15}$$

with $C_\Omega = 2.25$. Coefficients c_μ, q_i and c_i depend on the invariants:

$$S = \sqrt{2S_{ij}S_{ij}}, \quad \Omega = \sqrt{2\Omega_{ij}\Omega_{ij}} \tag{16}$$

and on the dimensionless combination:

$$\eta = \tau_t (S^2 + \Omega^2)^{1/2}. \tag{17}$$

The expression for c_μ is

$$c_\mu = \frac{1}{A_1 + A_s \eta + 25(1 - f_{R_y})W}, \tag{18}$$

with $A_1 = 4$, $A_s = \sqrt{3}\cos\phi$ and $\phi = \frac{1}{3}\arccos(\sqrt{6}W)$, with:

$$W = 2^{1.5}\frac{S_{ij}S_{jk}S_{ki}}{S^3}. \tag{19}$$

The final term in the denominator of Eq. (18) seriously improves the heat transfer predictions for turbulent impinging jets: it prevents overprediction of turbulent kinetic energy in stagnation regions. This term is practically negligible for all other flows in [9].

The coefficients q_1 and q_2 are

$$\begin{cases} q_1 = f_W(7 + 2.1\eta + 4.2 \times 10^{-3}\eta^3)^{-1} \\ q_2 = f_W(10 + 3.6\eta + 1 \times 10^{-2}\eta^3)^{-1} \end{cases}, \tag{20}$$

where f_W has been added for the case of turbulent impinging jets again:

$$f_W = 1 - 18W^2 + (72/\sqrt{6})W^3. \tag{21}$$

This function turns off the second-order terms in (14) in axisymmetric stagnation regions (where $W = 1/\sqrt{6}$). Consequently, the turbulent normal stress, perpendicular to the plate, is less overpredicted in the stagnation region. This will be further discussed during the description of the results. The coefficient c_1 is defined as

$$\begin{cases} S \geqslant \Omega : c_1 = -f_W \min(40c_\mu^4; 0.15) \\ S < \Omega : c_1 = -f_W \min(\min(600c_\mu^4; 0.15); \\ \quad 4f_\mu c_\mu/(\Omega^2\tau_t^2 - S^2\tau_t^2)). \end{cases} \tag{22}$$

Again, the introduction of f_W improves heat transfer results in stagnation regions. The polynomial for $S \geqslant \Omega$ is different from the one in [7], due to the different formulation for c_μ. The use of the factor 600 results in an overprediction of the destabilising effect of streamline curvature on turbulence. Since c_1 is the coefficient of a term which becomes zero for $S = \Omega$ in Eq. (14), there is no problem of discontinuity by the jump from factor 40 to 600 in expression (22). The coefficient c_2, which has some effect in swirling flows, is

$$c_2 = -2c_1. \tag{23}$$

The damping function f_μ is

$$f_\mu = 1 - \exp(-6 \times 10^{-2}\sqrt{R_y} - 2 \times 10^{-4}R_y^{1.5} - 2 \times 10^{-8}R_y^4), \tag{24}$$

with R_y as defined above.

To conclude, it is remarked that Eq. (14) does not contain a quadratic term in the vorticity tensor, since this would violate certain realizability conditions in rotating geometries [6]. In spite of this, many other models (e.g. [5]) still do contain such a term.

4. Numerical method

The steady-state solution is obtained through a time marching method with a finite volume technique. The spatial discretization is an AUSM-like second-order accurate scheme, in which acoustic and diffusion fluxes are discretized centrally and upwinding is used for the convective fluxes [17]. The treatment of the source terms in the turbulence transport equations is described in [18]. The higher order terms in the constitutive law (14) are treated partly implicitly (the second-order terms in the turbulent normal stresses) and partly explicitly (all other terms). A complete description of the numerical method is given in [10].

5. Results

5.1. Test case description

The geometry is depicted in Fig. 1. The turbulent air flow at the exit of the nozzle, with diameter D, is fully

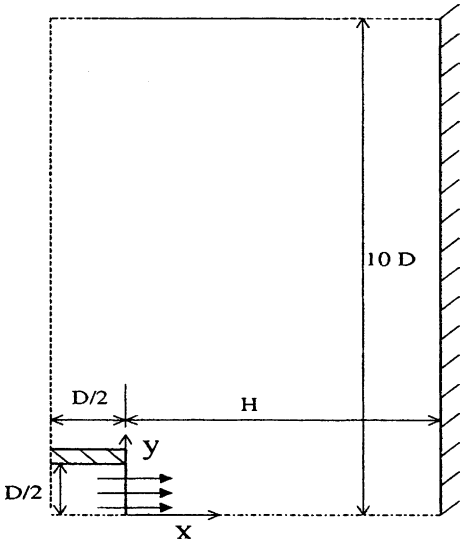

Fig. 1. Geometry and computational domain.

developed. The nozzle is at a distance H from the flat plate. The Reynolds number, based on the diameter and the bulk velocity U_b, is $Re = (\rho U_b D)/\mu = 23000$. A uniform small heat flux is imposed at the flat plate. Local heat transfer has been measured by Baughn et al., for different distances between the nozzle and the plate [11]. Later, more sets of experimental data have been established [12–14]. As mentioned in [3], there is significant spreading in the measured rates of heat transfer, although most investigators reported uncertainties of the order of 5%.

The flow field has also been studied experimentally [15]. The most elaborate set of data is available for $H = 2D$. Therefore, flow field results are presented for this configuration.

5.2. Computational grid

The computational grid, containing 129×113 points, starts $1/2D$ upstream of the nozzle exit. Consequently, the entrainment of the coflow air is correctly reproduced. There are 16 cells ahead of the nozzle exit, with refinement near the exit.

Radially, 40 cells lie within the pipe. The grid is refined near the symmetry axis (in order to have sufficient accuracy near the stagnation point) and at the edge of the nozzle (so that the entrainment is accurately described). Within the thickness of the pipe (equal to $0.0313D$ [3]), there are four equally sized cells. Radial stretching is applied to the upper boundary. Axially, the cell at the stagnation point is square. Also the cells at the nozzle within the pipe thickness are squares. Axial stretching is applied for all other cells.

All results with the present model have been checked to be grid independent by refining the grid in the two directions (not shown). At different positions in the field, the most important variables have been monitored on the original grid and on the refined grid and no differences larger than 0.1% have been observed between the solutions on both grids.

5.3. Boundary conditions

A fully developed turbulent pipe flow is imposed at the inlet boundary, while static pressure is extrapolated from the flow field. The coflow air is imposed, too: it is assumed to be a fully developed boundary layer flow with free stream velocity equal to 10% of the bulk pipe exit velocity. The turbulence level is set to 1%. The air entrainment is accurately described, since the inlet of the computational domain is sufficiently far upstream of the nozzle exit. The inlet air temperature is prescribed as 293 K.

At the flat plate, the velocity components and turbulent kinetic energy are set to zero. A zero derivative is used for the static pressure. The dissipation rate is determined as in [1]: $\varepsilon_w = 2(\mu/\rho)(\partial\sqrt{k}/\partial x)^2$. The temperature at the plate is prescribed as 313 K. It is noteworthy that this boundary condition differs from the experimental set-up, where a constant heat flux $|q_w|$ is imposed. As reported in [11], small temperature differences (in the order of 10 K) are observed, so that imposing a constant plate temperature is a good approximation. This numerically feasible boundary condition is used. Moreover, the resulting variable heat flux does not cause any problems, since, as stated in [11], the influence on the results for the Nusselt number, defined as

$$Nu = \frac{D|q_w|}{\kappa(T_w - T_0)} \tag{25}$$

is negligible, as long as the heat flux $|q_w|$ is sufficiently small. In the experiment, $|q_w|$ is constant and T_w is variable. Here, the plate temperature T_w is imposed and the heat flux is variable and Nu is determined as in [3]:

$$Nu = \frac{D\left|\frac{\partial(T-T_0)}{\partial x}\right|_{x=x_w}}{T_w - T_0} \tag{26}$$

with x_w the position of the plate and T_0 the air temperature at the nozzle exit. A test computation a posteriori with imposed small heat flux and Nu determined from (25) verified that the Nusselt number remains unchanged, compared to an imposed plate temperature.

All other boundary conditions are standard.

5.4. Nusselt number profiles

In Table 1, the Nusselt number at the stagnation point is given for distances $H = 2D$ and $6D$ between the nozzle and the flat plate. The predictions with the low-Reynolds standard k–ε model are unacceptable: the heat transfer is overpredicted by a factor of two. The v^2–f results [2] are in excellent agreement with the experimental data. The quality of the present model is very good, too, despite a small overprediction for $H = 2D$. In [2], the overprediction of the Nusselt number with the standard k–ε model is explained by the high level of turbulent kinetic energy, obtained with this model. Indeed, the standard k–ε model erroneously generates a spurious, amount of turbulent kinetic energy near the stagnation point (see later Figs. 4 and 5), while the v^2–f model does not [2]. However, the reason seems to be slightly more subtle, as can be learnt from Fig. 2. Part *a* of the figure shows the mean velocity along the symmetry axis. Agreement with experimental data is very

Table 1
Stagnation point Nusselt number for $H/D = 2$ and 6

Model	k–ε	v^2–f [2]	Present	Exp.
$H/D = 2$	312	150	154	135–150
$H/D = 6$	330	178	161	146–183

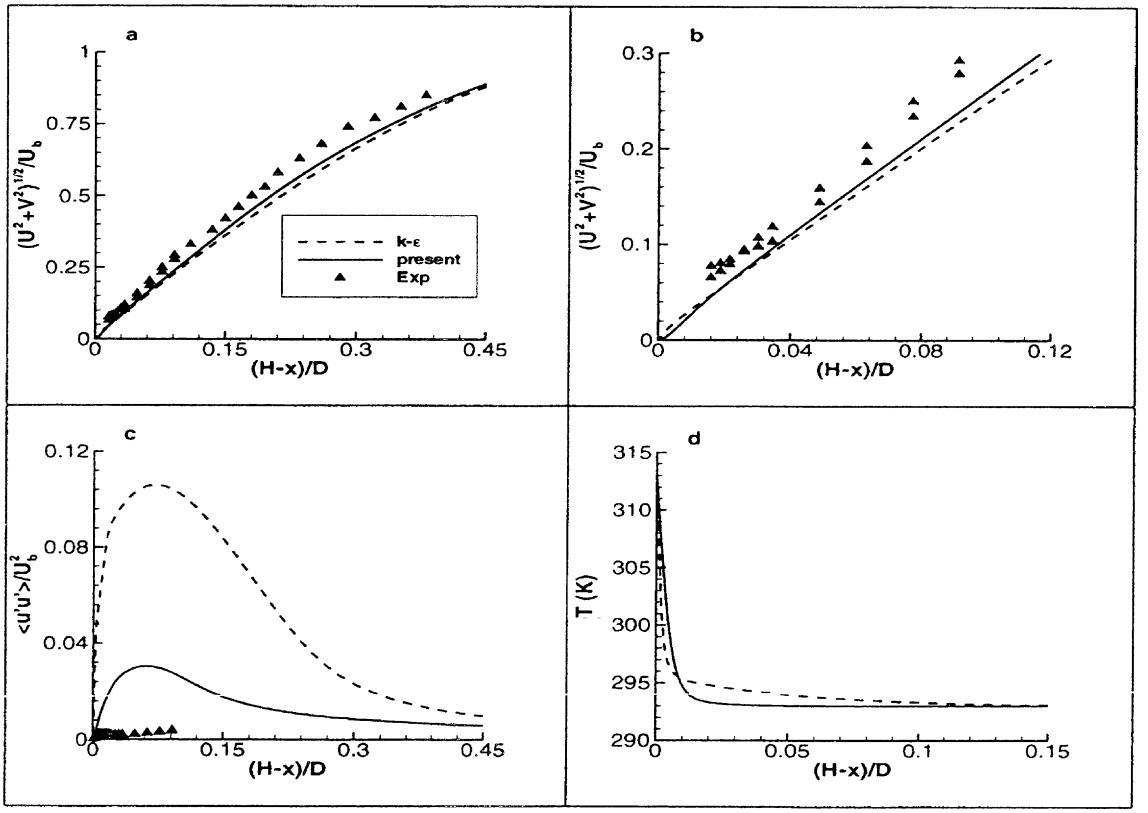

Fig. 2. Profiles on the symmetry axis for $H/D = 2$.

good, and at first sight, differences between the profiles for the YS model and the present model are negligible. However, the Nusselt number (25) is determined from the temperature gradient at the flat plate, which on its turn is determined by the velocity field near the stagnation point, since the mean temperature field is governed by a convection–diffusion equation (1). In part *b* of Fig. 2, this region is zoomed in at. It is seen that the velocity is lower with the YS model, except very close to the flat plate ($x < 0.02D$, with x the distance from the plate). The reason for this behaviour is seen in part *c* of Fig. 2, showing the turbulent normal stress at the axis. The axial derivative of this stress is an important quantity in the momentum-x equation. This is what actually counts: it is not directly the value of the turbulent normal stress (or the turbulent kinetic energy) which governs the flow field and thus determines the Nusselt number, but the resulting force of the stresses. Coming from the nozzle, the air stream decelerates towards the plate. When there is an increase in $\overline{u'u'}$, the deceleration is stronger due to the resulting force $(\partial\overline{u'u'})/(\partial x)$. Similarly, when there is a decrease in $\overline{u'u'}$, the deceleration is weaker. Looking at picture *c*, the increase in $\overline{u'u'}$ is observed farther away from the plate for the k–ε model than for the present model. The increase is also steeper. This explains the lower velocity with the YS model in pictures *a* and *b* sufficiently far from the plate. The peak in $\overline{u'u'}$ is much higher than with the present model (and orders of magnitude higher than experimentally measured), and the decrease behind the peak is much steeper than with the present model. This explains the higher velocity with the YS model for $x < 0.02D$. The axial velocity profile is of crucial importance for the value of the stagnation point Nusselt number. As already mentioned, Nu is determined from the mean temperature gradient, while the mean temperature field is governed by a convection–diffusion equation (1). The higher the velocity, the more important convection is, compared to the diffusion. Since the velocity with the YS model is lower than with the present model for $x > 0.02D$, and the turbulent viscosity (11) is higher due to higher levels of turbulent kinetic energy, diffusion of the temperature is more important. This explains, as seen in picture *d*, why the air temperature rises from $x \approx 0.12D$, while with the present model the increase is postponed until $x \approx 0.02D$. Still the temperature gradient at the plate is much higher with the YS model, due to the higher velocity with the YS model for $x < 0.02D$: convection is relatively more important, compared to diffusion, than with the present model,

resulting in a steeper mean temperature gradient and a higher Nusselt number. It is noteworthy that the v^2–f model yields excellent agreement with the experimental data for $\overline{u'u'}$ [2], while with the present model this stress is still overpredicted. This confirms the statement that the reason for the high Nusselt number with the YS model is not solely related to a spurious amount of turbulent kinetic energy, since the present model still suffers from some (be it less pronounced) overprediction. However, this is not dramatic, since it is the resulting force of the normal stress which is important, rather than the amount of turbulent kinetic energy, as explained above. The prediction of $\overline{u'u'}$ can thus be thought of as 'aesthetic', rather than fundamental.

With respect to the accuracy of the prediction of the stagnation point Nusselt number, different aspects of the present model are important. Firstly, there is definition (18) of c_μ. In particular the final term in the denominator ensures that the overprediction of the turbulent kinetic energy becomes less pronounced. This has a beneficial effect on the axial derivatives of the normal turbulent stress, resulting in better Nusselt number predictions, as explained above. It is noteworthy that $W = 1/\sqrt{6}$ in the stagnation region activates this final term, while the factor $(1 - f_{R_y})$ makes sure that the term is zero away from solid boundaries. It is also noteworthy that in [5], a similar, but more complex, term is added in the denominator of the expression for c_μ, for the same reason, namely to reduce the production of turbulent kinetic energy. The second important aspect is the introduction of the term (13) in the ε-equation (5). In [10], the effect of this term has been illustrated for the YS model. The prediction of the stagnation point Nusselt number is seriously improved ($Nu = 183$ instead of $Nu = 312$ for $H = 2D$ and $Nu = 202$ instead of $Nu = 330$ for $H = 6D$). With the present model, it is the combination of term (13) in the ε-equation with the definition of c_μ which form the basis for the good Nusselt number predictions. The third aspect is the introduction of factor f_W (21) into the higher order terms (20) and (22) in the constitutive law (14). Since $W = 1/\sqrt{6}$ in the stagnation region implies that f_W becomes zero, the higher order terms are set to zero. For the second-order terms, the effect is a lower peak for $\overline{u'u'}$ for a certain amount of turbulent kinetic energy, resulting in lower values for the axial derivatives, with the beneficial effect as described above. For the term multiplied by c_1, this implies a lower level of turbulent kinetic energy: when $S > \Omega$, as is the case at the symmetry axis, the term with c_1 in (14) has the effect of increasing the turbulent kinetic energy [7]. By setting c_1 to zero, this is avoided. The relatively lower value of turbulent kinetic energy also reduces the peak in $\overline{u'u'}$.

So far, the discussion has been restricted to the stagnation point Nusselt number. In Fig. 3, the profiles of Nu at the plate are shown for $H = 2D$ and $6D$. For $H = 2D$, a secondary maximum is observed experimentally at $r \approx 2D$, while such a secondary maximum is absent for $H = 6D$. In [2], it is reported that the v^2–f model does not predict this secondary maximum (a deflection point is obtained in the profile). With the present model, the behaviour is exactly reproduced. Even the position of the secondary maximum for $H = 2D$ is correct. Globally, the Nusselt number is somewhat underpredicted for large r. In general, the quality of the Nusselt number profiles is for both distances comparable to what is shown for the v^2–f model in [2,3]. As was also shown in [2], the results with the k–ε model are reasonable for larger r. The values for Nu with the YS model are slightly lower in Fig. 3 than reported in [2]. This is probably due to the low-Reynolds formulation of the model here.

The correct prediction of the secondary maximum for $H = 2D$ and the absence hereof for $H = 6D$ is due to the formulation (18) of c_μ: in [10] it was illustrated that the introduction of term (13) in the ε-equation improves the value of the stagnation point Nusselt number, but does not lead to the prediction of the secondary maximum of Nu for $H = 2D$.

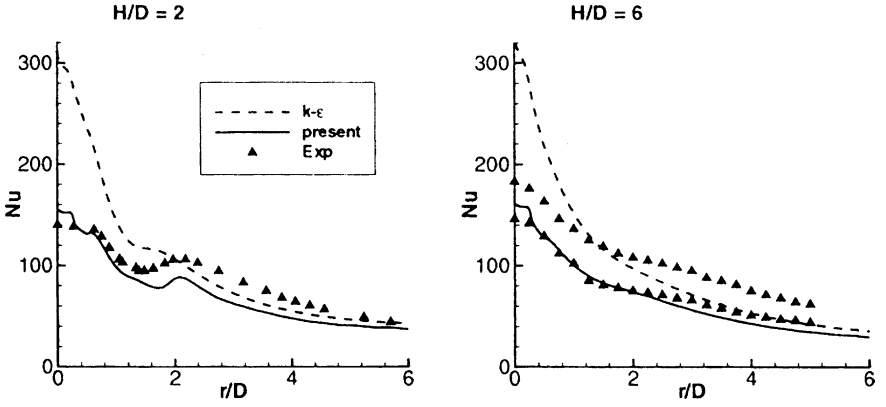

Fig. 3. Nusselt number profiles at the flat plate for $H/D = 2$ and $H/D = 6$.

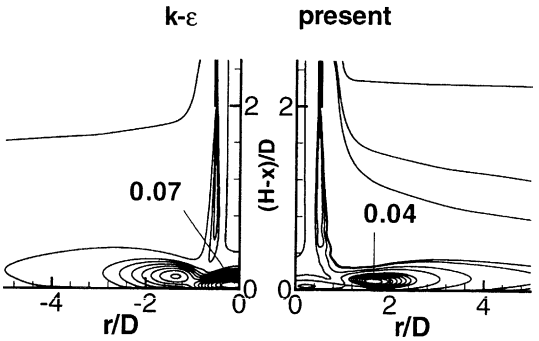

Fig. 4. Fields of turbulent kinetic energy, normalised by U_b^2, for $H/D = 2$.

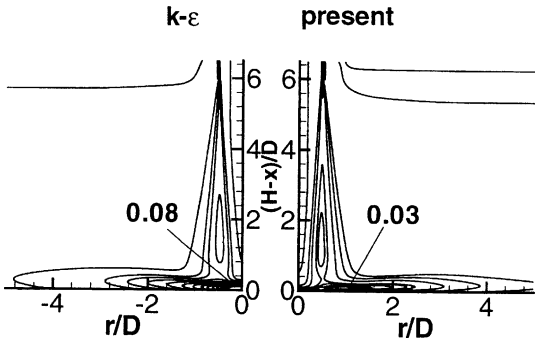

Fig. 5. Fields of turbulent kinetic energy, normalised by U_b^2, for $H/D = 6$.

In [2], the existence of the secondary maximum in Nu is attributed to the off-axis position of the maximum in turbulent kinetic energy. It is reported that, with the standard k–ε model, the maximum turbulent kinetic energy is erroneously predicted to lie on the axis for both $H = 2D$ and $6D$, while with the v^2–f model, the positions for the maximum turbulent kinetic energy are at $r \approx 2D$ and $\approx 1D$ respectively. In Figs. 4 and 5, the fields of turbulent kinetic energy, obtained with the YS model and with the present model, are shown similarly as was done in [2]. It is observed that the maximum values with the YS model indeed lie on the axis, while with the

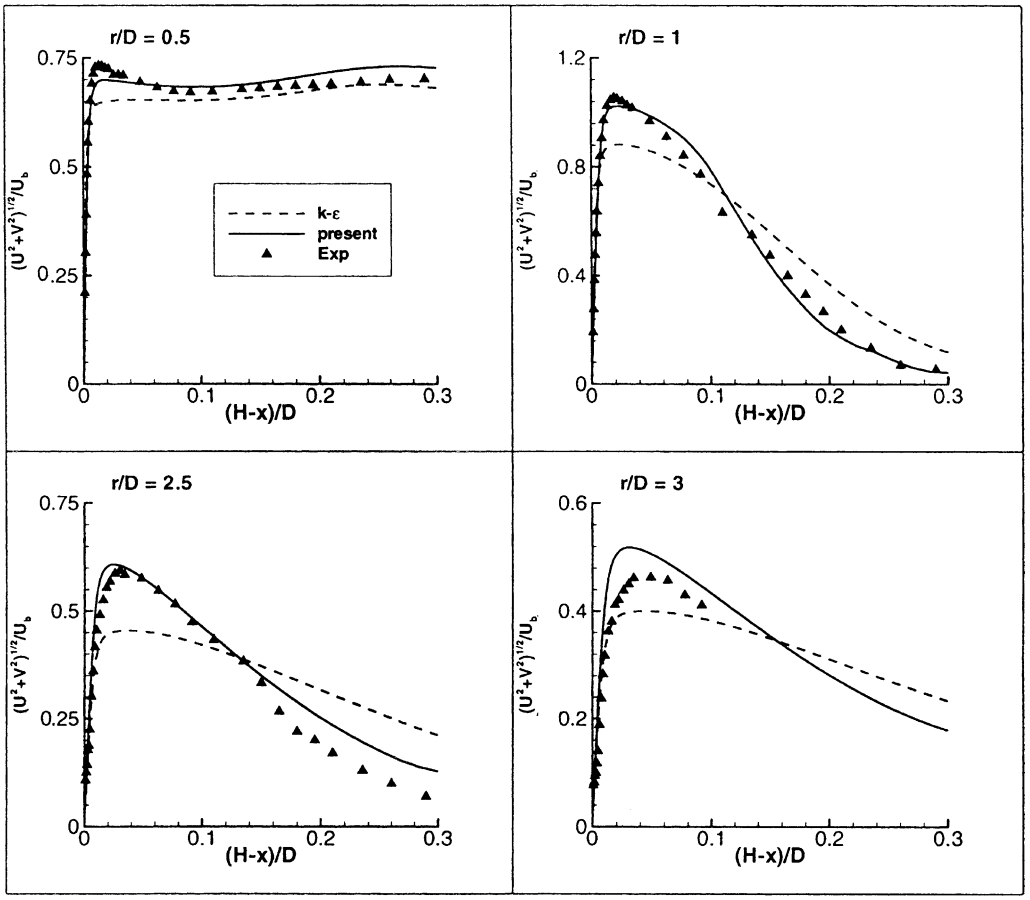

Fig. 6. Mean velocity profiles at different radial positions for $H/D = 2$.

present model the positions are almost identical to the results with the v^2–f model. This illustrates that with the present model, qualitatively very similar results are obtained as with the v^2–f model. The values of the maxima are slightly lower than reported in [2], probably due to the low-Reynolds formulation of the models in this work. It is noted that, as in [2], the maximum k is much higher with the YS model than with the present model. Finally, it is noted that, as already stated above, the Nusselt number is not directly related to the level of turbulent kinetic energy. For both distances, the maximum k is not obtained on the axis with the present model, while the maximum Nusselt number is reached at the stagnation point. Again, this illustrates that the reasoning for Nusselt numbers is more subtle than simply based on the level of turbulent kinetic energy. It is the resulting flow field which is the most important.

5.5. Flow field predictions

The flow field was studied experimentally by Cooper et al. [15]. An extensive data set is available for $H = 2D$, so that the discussion is restricted to this configuration. As explained above, the flow field prediction forms the basis for accurate Nusselt number profiles.

In Fig. 6, the mean velocity profiles are shown for different radial positions. As reported in [2], the standard k–ε model predicts too low velocities for $r = 0.5D$, and the flow acceleration towards $r = D$ is badly reproduced: the velocities are too low in the wall region and too high in the outer region. With the present model, agreement with the experimental data is excellent: the flow acceleration is well described. Going further radially outward, the flow deceleration and development of a boundary layer are very well predicted with the present

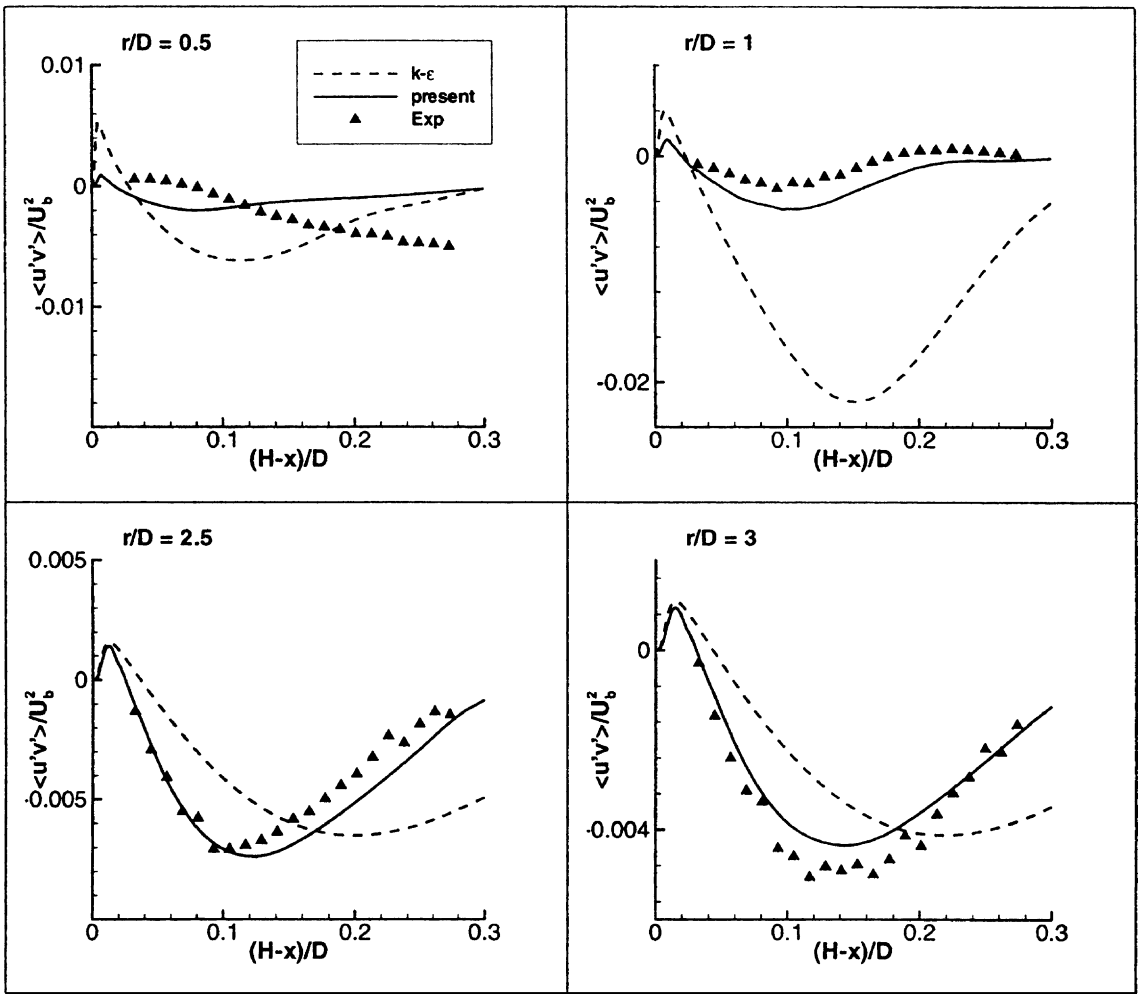

Fig. 7. Profiles of turbulent shear stress at different radial positions for $H/D = 2$.

model, with excellent agreement for $r = 2.5D$ and a slight overprediction at $r = 3D$. With the YS model, the velocity is far too low near the wall and too high in the outer region. The quality of the mean velocity profiles is closely related to the turbulent shear stress profiles, since their resulting force is the largest contribution in the momentum equations (outside the stagnation region $r < 0.5D$). In Fig. 7 it is illustrated that agreement with experimental data is excellent with the present model (except for $r = 0.5D$). This quality is due to both the ε-equation (5) and the constitutive law (14), in particular the definition (18) for c_μ. With the YS model, agreement is much less satisfactory.

To conclude the discussion of the flow field, profiles for the turbulent normal stresses are shown in Fig. 8. Again, it is seen that agreement between the results of the present model and the experiments is satisfactory, in contrast to the YS model results. Both the level of turbulent kinetic energy and the distribution to the different normal stresses (through the second-order terms in Eq. (14)) contribute to the quality of the normal stress profiles.

5.6. Effect of nozzle distance

In Table 2, the effect on the stagnation point Nusselt number of the distance between the nozzle exit and the plate, is illustrated. Comparisons are made to experimental data, the YS model and the v^2–f model. Clearly, the quality of the results with the present model is very good, comparable to the v^2–f model. This illustrates the good behaviour of the present model for different geometry configurations.

5.7. Effect of Reynolds number

In Fig. 9, values of the stagnation point Nusselt number are shown for $H/D = 6$ for different Reynolds

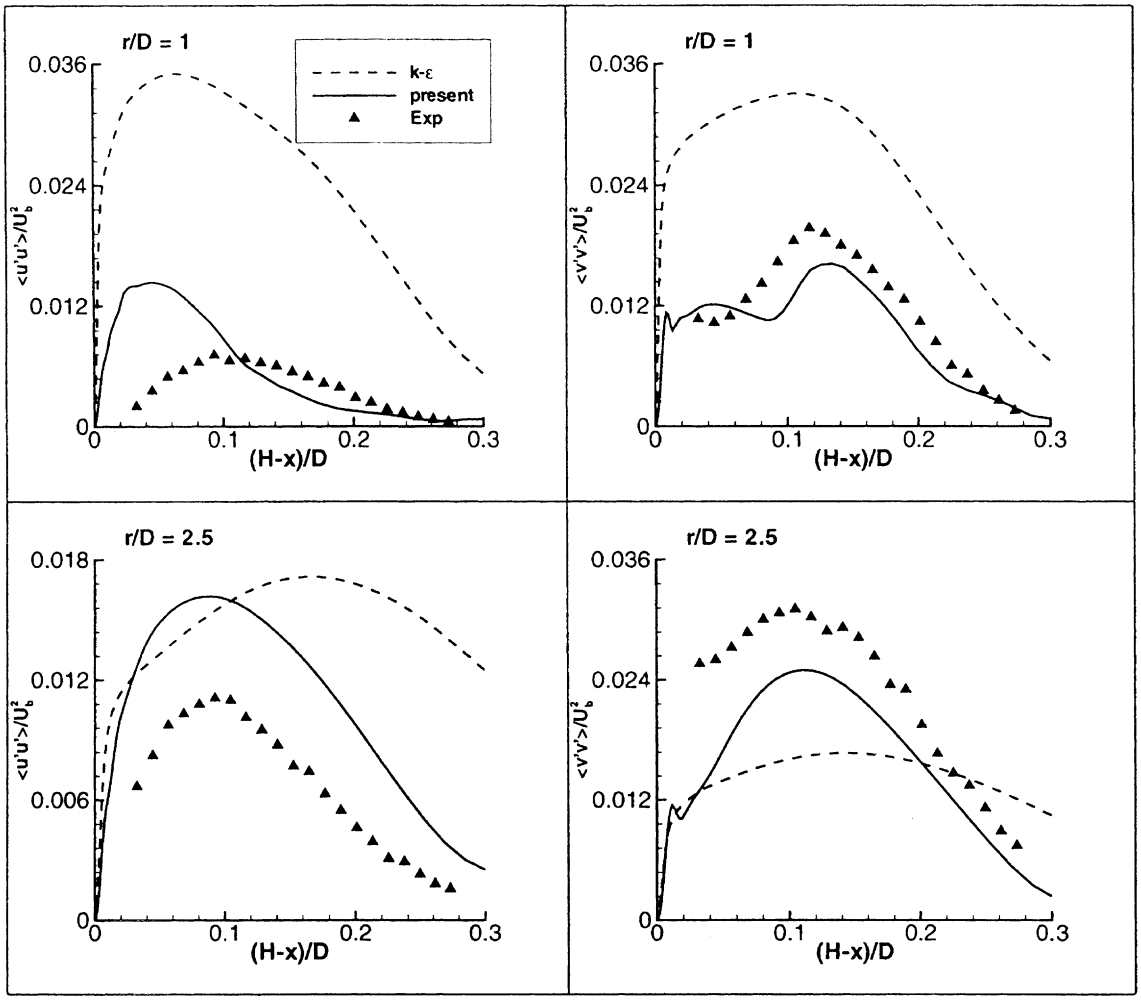

Fig. 8. Profiles of turbulent normal stresses at different radial positions for $H/D = 2$.

Table 2
Influence of nozzle distance on stagnation point Nusselt number

H/D	1	2	4	6	10	14
k–ε	225	312	243	330	270	180
v^2–f [2]	151	150	153	178	135	94
Present	157	154	145	161	160	105
Exp.	170	135–150	135	146–183	130–151	108

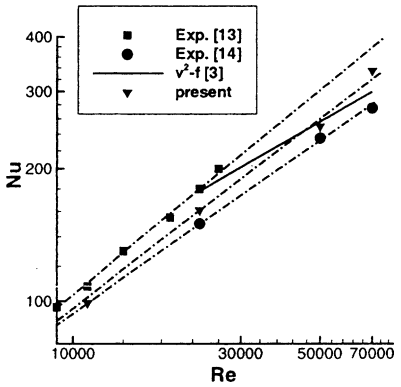

Fig. 9. Influence of Reynolds number on the stagnation point Nusselt number for $H/D = 6$.

Table 3
Value of exponent m in the relation $Nu_{stag} \sim Re^m$

Data set	Exp. [13]	Exp. [14]	v^2–f [3]	Present
Exponent	0.55	0.68	0.5	0.62

numbers. Best line fits are drawn for the two sets of experimental data [13,14] and the results with the present model. The solid line denotes the v^2–f results of [3].

Since straight lines are obtained in the log–log diagram, it is seen that $Nu_{stag} \sim Re^m$. In Table 3, the exponent m is given for the two sets of experimental data, the v^2–f model and the present model. It is seen that the exponent $m = 0.62$ of the present model is well within the experimentally obtained values of exponents. It is noted that in [3], a single exponent $m = 0.5$ is reported when a best line fit is drawn for both sets of experimental data together. However, when the influence of a parameter, i.e. the Reynolds number, is studied, it is more reasonable to consider both sets of experimental data separately. This guarantees that the only influence factor on the results is the examined variation of the studied parameter.

6. Discussion

It is well known that the v^2–f model produces excellent results for the considered test case [2,3]. The purpose of this paper is not to present a model that outperforms the v^2–f model, but to show that there is some potential in non-linear two-equation turbulence models in heat transfer calculations with impinging flows. In fact, this has already been done in [5], but the proposed model contains a quadratic vorticity term in the constitutive law that violates certain realizability constraints, and the model has been tuned specifically for the heat transfer test cases of that paper. The model presented here, has some advantages, since it does not contain the mentioned second-order terms and it has already been applied to a variety of flows in the current formulation [9].

7. Conclusions

Results have been presented for the turbulent heat transfer in axisymmetric jets, impinging onto a flat plate, with a low-Reynolds non-linear k–ε model.

The heat transfer, expressed in terms of Nusselt numbers, is very well predicted. The stagnation point Nusselt number is in excellent agreement with experimental data, for a wide range of distances between the nozzle exit and the plate ($H = 1D$ to $14D$). This is due to both definition (18) of c_μ and the term (13) in the ε-equation (5). It was explained that in the stagnation region, the resulting force of the turbulent normal stress, perpendicular to the plate, is the cause for good or bad predictions of the stagnation point Nusselt number. The two mentioned aspects of the model counteract the erroneous overprediction of turbulent kinetic energy by the standard k–ε model and lead to better resulting turbulent normal stress forces.

Moreover, the qualitative behaviour of the model is correct for the Nusselt number profiles at the plate. For the distance $H = 2D$, the experimentally observed secondary maximum in the Nusselt number profile is well predicted at the correct radial position. For the distance $H = 6D$, no secondary maximum is observed, and it is not predicted, either. This quality is mainly due to definition (18) of c_μ.

Accurate flow field predictions form the basis for good Nusselt number profiles at the plate. It was illustrated, for $H = 2D$, that excellent agreement is obtained between the mean velocity profiles of the present model and experimental data at different radial positions. Both the non-linear expression (14) and the ε-equation (5) have a contribution. The main reason for the excellent agreement is the accurate prediction of the turbulent shear stress, which is the most important one outside the stagnation region. With the present model, this stress is well reproduced, as are the turbulent normal stresses.

For a fixed Reynolds number, the influence of the distance between the nozzle exit and the flat plate on the stagnation point Nusselt number is captured well. For a

fixed nozzle–plate distance, the effect of the Reynolds number is correctly reproduced. This indicates the general validity of the present model.

Acknowledgement

The first author is a Postdoctoral Fellow of the Fund for Scientific Research—Flanders (Belgium) (F.W.O. Vlaanderen).

References

[1] Z.Y. Yang, T.H. Shih, A new time scale based k–ϵ model for near-wall turbulence, AIAA J. 31 (7) (1993) 1191–1198.
[2] M. Behnia, S. Parneix, P.A. Durbin, Prediction of heat transfer in an axisymmetric turbulent jet impinging on a flat plate, Int. J. Heat Mass Transfer 41 (12) (1998) 1845–1855.
[3] M. Behnia, S. Parneix, Y. Shabany, P.A. Durbin, Numerical study of turbulent heat transfer in confined and unconfined impinging jets, Int. J. Heat Fluid Flow 20 (1999) 1–9.
[4] P. Durbin, Near-wall turbulence closure without damping functions, Theor. Comput. Fluid Dyn. 3 (1991) 1–13.
[5] T.J. Craft, H. Iacovides, J.H. Yoon, Progress in the use of non-linear two-equation models in the computation of convective heat-transfer in impinging and separated flows, Flow Turbul. Combust. 63 (2000) 59–80.
[6] C.G. Speziale, B.A. Younis, R. Rubinstein, Y. Zhou, On consistency conditions for rotating turbulent flows, Phys. Fluids 10 (8) (1998) 2108–2110.
[7] B. Merci, C. De Langhe, J. Vierendeels, E. Dick, A quasi-realizable cubic low-Reynolds Eddy-viscosity turbulence model with a new dissipation rate equation, Flow Turbul. Combust. 66 (2) (2001) 133–157.
[8] B. Merci, E. Dick, J. Vierendeels, D. Roekaerts, T.W.J. Peeters, Application of a new cubic turbulence model to piloted and bluff-body diffusion flames, Combust. Flame 126 (1–2) (2001) 1533–1556.
[9] B, Merci, E. Dick, Predictive capabilities of an improved cubic k–ε model for inert steady flows, Flow Turbul. Combust., in press.
[10] B. Merci, J. Vierendeels, C. De Langhe, E. Dick, Numerical simulation of heat transfer of turbulent impinging jets with two-equation turbulence models, Int. J. Numer. Meth. Heat Fluid Flow, in press.
[11] J.W. Baughn, S. Shimizu, Heat transfer measurements from a surface with uniform heat flux and an impinging jet, J. Heat Transfer 111 (1989) 1096–1098.
[12] J.W. Baughn, A. Hechanova, X. Yan, An experimental study of entrainment effects on the heat transfer from a flat surface to a heated circular impinging jet, J. Heat Transfer 113 (4) (1991) 1023–1025.
[13] X. Yan, A Preheated-Wall Transient Method Using Liquid Crystals for the Measurement of Heat Transfer on External Surfaces and in Ducts, PhD Thesis, University of California, Davis, 1993.
[14] D. Lytle, B. Webb, Air jet impingement heat transfer at low nozzle–plate spaces, Int. J. Heat Mass Transfer 37 (12) (1994) 1687–1697.
[15] D. Cooper, D.C. Jackson, B.E. Launder, G.X. Liao, Impinging jet studies for turbulence model assessment—I. Flow field experiments, Int. J. Heat Mass Transfer 36 (10) (1993) 2675–2684.
[16] T.H. Shih, W.W. Liou, A. Shabbir, Z. Yang, J. Zhu, A new k–ε Eddy viscosity model for high Reynolds number turbulent flows, Comput. Fluids 23 (3) (1995) 227–238.
[17] J. Vierendeels, B. Merci, E. Dick, A blended AUSM+ method for all speeds and all grid aspect ratios, AIAA J. 39 (12) (2001) 2278–2282.
[18] B. Merci, J. Steelant, J. Vierendeels, K. Riemslagh, E. Dick, Computational treatment of source terms in two-equation turbulence models, AIAA J. 38 (11) (2000) 2085–2093.